Large-scale mapping of live corals to guide reef conservation

Gregory P. Asner[a,b,1], Nicholas R. Vaughn[a,b], Joseph Heckler[a,b], David E. Knapp[a,b], Christopher Balzotti[a,b], Ethan Shafron[a,b], Roberta E. Martin[a,b], Brian J. Neilson[c], and Jamison M. Gove[d]

[a]Center for Global Discovery and Conservation Science, Arizona State University, Tempe, AZ 85281; [b]Center for Global Discovery and Conservation Science, Arizona State University, Hilo, HI 96720; [c]Division of Aquatic Resources, Department of Land and Natural Resources, State of Hawaii, Honolulu, HI 96813; and [d]Pacific Islands Fisheries Science Center, National Oceanic and Atmospheric Administration, Honolulu, HI 96818

Contributed by Gregory P. Asner, October 19, 2020 (sent for review August 20, 2020; reviewed by Russell E. Brainard and John Burns)

Coral is the life-form that underpins the habitat of most tropical reef ecosystems, thereby supporting biological diversity throughout the marine realm. Coral reefs are undergoing rapid change from ocean warming and nearshore human activities, compromising a myriad of services provided to societies including coastal protection, fishing, and cultural practices. In the face of these challenges, large-scale operational mapping of live coral cover within and across reef ecosystems could provide more opportunities to address reef protection, resilience, and restoration at broad management- and policy-relevant scales. We developed an airborne mapping approach combining laser-guided imaging spectroscopy and deep learning models to quantify, at a large archipelago scale, the geographic distribution of live corals to 16-m water depth throughout the main Hawaiian islands. Airborne estimates of live coral cover were highly correlated with field-based estimates of live coral cover (R^2 = 0.94). Our maps were used to assess the relative condition of reefs based on live coral, and to identify potential coral refugia in the face of human-driven stressors, including marine heat waves. Geospatial modeling revealed that water depth, wave power, and nearshore development accounted for the majority (>60%) of live coral cover variation, but other human-driven factors were also important. Mapped interisland and intraisland variation in live coral location improves our understanding of reef geography and its human impacts, thereby guiding environmental management for reef resiliency.

coral mapping | coral reef | coral refugia | Hawaiian Islands | reef restoration

Coral is the foundational, habitat-generating life-form of most tropical reefs, but coral is under increasing pressure from marine heat waves, coastal development, and resource extraction (1). Coral change is occurring at multiple ecological scales ranging from genotypic- and species-level responses to broad reef- and regional-level reorganization (2). However, the spatially continuous distribution of live coral cover remains unknown, owing to a scale gap between field and drone-based surveys that sample portions of any given reef and satellite-based approaches that fail to resolve live coral cover from space (3). This gap makes it difficult to map very large regions, such as island archipelagos, at the spatial and biological resolution of the habitat-forming organisms inhabiting these regions.

Operational mapping of live coral cover within and across reef ecosystems could provide opportunities for science and management to better address reef protection, resilience, and restoration. For example, reef areas with live coral cover persisting after repeated stressors, such as marine heat waves, may indicate coral refugia (4). Spatial information on refugia may then drive innovations in marine protection as well as scientific investigation of underlying drivers of coral survival (5). In turn, new understanding of survivorship may alter predictions of reef change in the current and forthcoming ocean climate (6, 7). Large-scale information on live coral cover can also inform restoration efforts. Reefs that have lost coral cover from activities such as coastal development could be targeted for restoration if these activities are curtailed. However, low coral cover reefs previously exposed to repeated marine heat waves and severe degradation may represent intractable restoration possibilities (8).

The eight main Hawaiian islands (MHIs) are an iconic case in point of regional variability in the face of multiple stressors. Human pressure on Hawaiian reefs is wide-ranging, from relatively low impact on Kahoʻolawe to high impact on Oʻahu (9). Coastal development has resulted in hot spots of sedimentation, waterborne pollutants, and reef removal, while fishing and other resource uses have generated declines in reef resilience (10). In parallel, a series of marine heat waves has nonuniformly engulfed the MHIs, with the 2014, 2015, and 2019 bleaching events being the most recent. The 2015 event generated live coral losses reaching more than 50% in some areas, but the geographic extent of loss or resistance remains unknown (11).

The MHIs span a latitude and longitude range of 4° and 6°, respectively, and vary in geologic age, from less than a few years old on parts of Hawaiʻi Island to more than six million years old on Niʻihau (12). Island age is accompanied by stage of accretion and subsidence, processes that generate enormous interisland and intraisland variation in reef extent associated with benthic substrate availability. Combined geophysical and anthropogenic variability across the MHIs has generated ecological complexity in reef composition common to reef systems worldwide.

Significance

Coral reefs are changing at unprecedented rates, and the majority of reefs are undergoing widespread losses in live coral cover. Management and policy development efforts focused on conserving and restoring coral reefs are hampered by a lack of geographically consistent and actionable high-resolution information on the specific location and extent of live coral. Based on an operational airborne technique, we developed and applied a live coral mapping capability across the main Hawaiian islands to identify potential coral refugia as well as reefs for potential coral restoration. Our findings inform current management actions across the archipelago and demonstrate the tactical role that live coral mapping can play to support decision-making at large ecological scales.

Author contributions: G.P.A., N.R.V., and J.M.G. designed research; G.P.A., N.R.V., J.H., D.E.K., C.B., E.S., R.E.M., and B.J.N. performed research; N.R.V. contributed new reagents/analytic tools; G.P.A. and N.R.V. analyzed data; and G.P.A., N.R.V., R.E.M., B.J.N., and J.M.G. wrote the paper.

Reviewers: R.E.B., King Abdullah University of Science and Technology; and J.B., University of Hawaii.

The authors declare no competing interest.

[1]To whom correspondence may be addressed. Email: gregasner@asu.edu.

This article contains supporting information online at https://www.pnas.org/lookup/suppl/doi:10.1073/pnas.2017628117/-/DCSupplemental.

First published December 14, 2020.

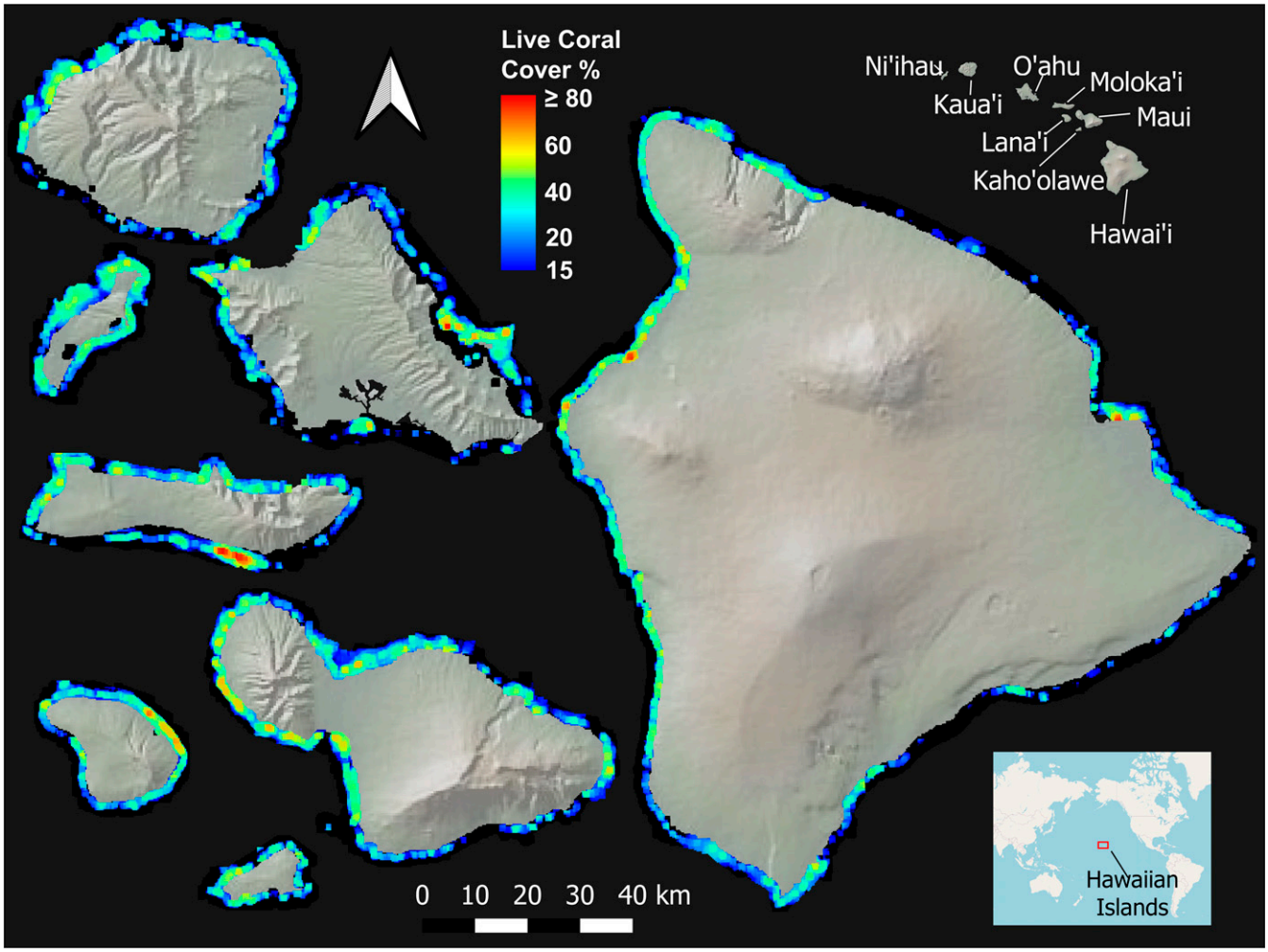

Fig. 1. Percent live coral cover at 2-m spatial resolution to 16-m depth for the eight Main Hawaiian Islands.

To assess land–sea controls over live coral cover, and to expand options for coral conservation and management, we undertook the first large-scale, high-resolution mapping study of live coral cover across an island archipelago. While there have been extensive in-water surveys of coral reefs in the MHIs, these have been constrained by site access and benthic variability, making the use of field information a challenge to the development of comprehensive regional maps of where live coral exists. Moreover, most airborne or satellite-based approaches derive benthic composition as aggregate classes such as coral combined with algal cover (e.g., refs. 13 and 14), and no programs have operationalized a method to cover large areas (e.g., >1,000 ha) with highly automated mapping of live coral location. We developed an airborne mapping approach that combines laser-guided imaging spectroscopy and computational deep learning to quantify the geographic distribution of live corals to a depth of 16 m. The resulting map was used to assess the relative condition of reefs from a coral perspective, and to identify areas of high live coral

Table 1. Inventory of reef cover and composition in the eight Main Hawaiian Islands in 2019 at 2-m spatial resolution to a water depth of 16 m

Island	Live coral cover, ha	Algal cover, ha	Sand cover, ha	Reef substrate, ha	Mapped area, ha
Ni'ihau	498 [10.0]	2,637 [9.0]	1,855 [6.6]	3,136	4,991
Kaua'i	552 [11.1]	3,162 [10.8]	4,117 [14.7]	3,715	7,831
O'ahu	1,164 [23.4]	8,836 [30.1]	11,698 [41.8]	10,001	21,699
Moloka'i	626 [12.6]	3,870 [13.2]	4,451 [15.9]	4,497	8,948
Lana'i	279 [5.6]	1,388 [4.7]	783 [2.8]	1,668	2,451
Maui	850 [17.1]	4,480 [15.2]	2,480 [8.9]	5,331	7,811
Kaho'olawe	90 [1.8]	461 [1.6]	302 [1.1]	553	855
Hawai'i	922 [18.5]	4,564 [15.5]	2,276 [8.1]	5,486	7,762
Total	4,984	29,401	27,964	34,386	62,350

The brackets indicate the proportional contribution of each island to the entire inventory of live coral, algal cover, and sand cover throughout the mapping coverage. Reef substrate is live coral cover plus algal cover. Total mapped area is the sum of live coral, algal cover, and sand cover.

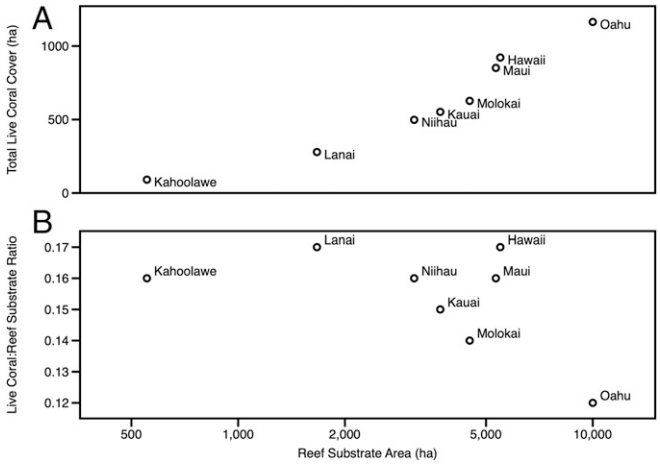

Fig. 2. Island-scale relationships between reef substrate area (in hectares) and (*A*) total live coral cover (in hectares) and (*B*) ratio of live coral cover to reef substrate availability.

cover, deemed potential refugia. Following geospatial analyses of live corals, we used computational machine learning to quantify multiple land–sea drivers affecting live coral cover, as a means to inform mitigation and restoration efforts throughout the MHIs.

Results

Interisland Reef Composition. Across the MHIs, the total shallow reef area mapped was 62,350 ha covering about 95% of all known reefs to a depth of 16 m (Fig. 1, Table 1, and *SI Appendix*, Figs. S1 and S2). Of that mapped area, 34,386 ha are composed of either live coral or algal cover (including algae on rock surfaces), which combined, we refer to here as "reef substrate" that excludes open sand cover. Just 15% (4,984 ha) of reef substrate is currently covered in live coral throughout the main archipelago. In terms of live coral cover contributions to the MHIs, the top three islands are Oʻahu (23.4% of MHI coral), Hawaiʻi (18.5%), and Maui (17.1%), which collectively account for 60% of all live coral cover (Table 1 and Fig. 2*A*). However, algal cover is also highest off Oʻahu, resulting in the lowest proportion of live coral (12%) per unit reef substrate in the main archipelago (Fig. 2*B*). The second largest system is the fringing reef of Hawaiʻi Island, which covers 5,486 ha of reef substrate, with 922 ha (17%) of this area comprising live coral. On a reef substrate basis, Hawaiʻi Island has proportionally more live coral than any other island, and 42% more than the lowest ranking island of Oʻahu (Fig. 2*B*).

Coral Mapping Validation. Field-measured live coral cover was highly correlated with live coral estimates derived from airborne mapping (R^2 = 0.94; Fig. 3 and *SI Appendix*, Fig. S3). The root-mean-squared error (RMSE) between field and airborne results was 0.08, with 6% and 11% of the 1132 field transects falling beyond one and two RMSE units, respectively, from the 1:1 line against airborne measurements. In most cases, points of disagreement fell above the 1:1 line, indicating that the airborne method underestimates more often than overestimates live coral cover. There was no significant difference in validation results between windward and leeward field sites (*SI Appendix*, Fig. S4), reducing concern that the performance of the mapping could be disproportionally affected by windward coastlines with typically stronger winds and larger waves.

Geospatial Variation in Live Coral. Live coral cover showed a highly variable spatial arrangement at intraisland and interisland scales (Fig. 4). Variogram-range maps revealed that most reefs contain live coral cover that varies at high spatial frequency, often less than 100 m, indicated by low range values (Fig. 4*A*). However, this background condition is punctuated by stretches of reef with relatively uniform live coral cover. Importantly, large stretches of reef along Oʻahu and Kauaʻi show high variogram-range values because live coral cover is consistently low. By contrast, Hawaiʻi Island is characterized by high-frequency shifts in live coral cover along nearly all of its coastline, where live coral cover is proportionally much higher (Fig. 2). Variogram-sills represent the baseline variation in live coral cover between areas on an island that are far enough apart to lack any shared local environmental controls. Oʻahu is largely uniform with the exception of Kaneʻohe Bay in the northeast and northwestern portions of the island (Fig. 4*B*). In contrast, Lanaʻi and Kahoʻolawe are among the most variable in terms of live coral cover (Fig. 4*C*).

Live Coral Hot Spots. We identified 20 reef sites ranked by live coral cover, each over a contiguous area of at least 10 ha, across the main archipelago (Fig. 5*A*). The highest density of live coral hot spots occurs on Hawaiʻi Island, followed by Maui, Kahoʻolawe, Molokaʻi, and Lanaʻi. A single hot spot of high coral cover was also found on Oʻahu and Niʻihau. Kauaʻi failed to make the top 20 live coral hot spots.

Among the top sites with the highest live coral cover areas, seven occur along Hawaiʻi Island, with five of those along the leeward west Hawaiʻi shoreline and two near the city of Hilo on east Hawaiʻi Island (*SI Appendix*, Table S1). Based on absolute live coral cover, the top site is Kīholo Bay, averaging about 33% live coral cover off NW Hawaiʻi Island (Fig. 5*B*). Another standout is Pāpā Bay, based partly on average coral cover (27%), but particularly in terms of coral cover uniformity, with a spatial SD of live coral cover of just 13% (*SI Appendix*, Table S1). Independent of coral cover uniformity, each of the topmost 10 sites contain subsections of reef with at least 1 ha of reef exceeding 80% live coral cover.

Live Coral Drivers. Our machine learning analyses revealed multiple contributors to the spatial distribution of live corals throughout the MHIs (Fig. 6). The model accounted for 90% of the overall geospatial variation in live coral cover, indicating that the land–sea variables used in the model were appropriate in explaining the live coral map. Many of the factors included in the model were measurably important to model accuracy, but water depth, maximum wave power, and nearshore development exerted the strongest influence (permutation reduced model R^2 by 0.62,

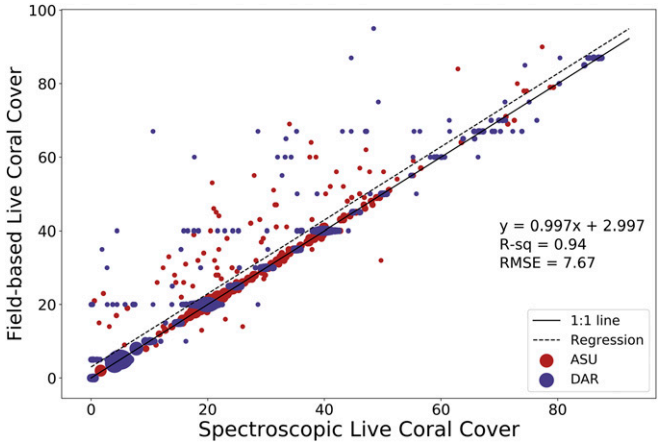

Fig. 3. Field verification of airborne live coral cover mapping across four Hawaiian islands (n = 1,132 transects). ASU, Arizona State University field sites; DAR, State of Hawaii Division of Aquatic Resources field sites.

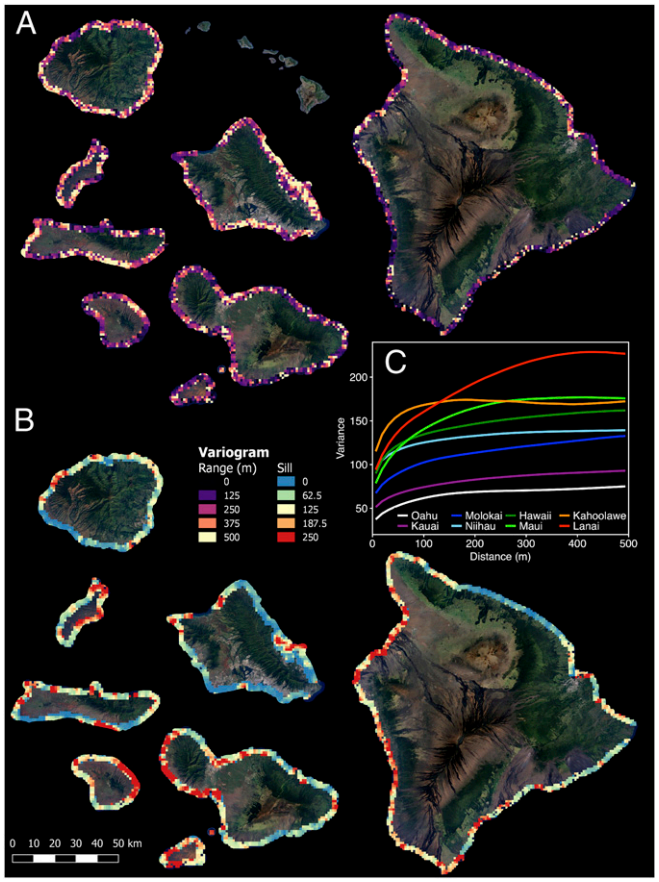

Fig. 4. Geospatial variation in live coral cover for the Main Hawaiian Islands. Semivariogram (*A*) range and (*B*) sill are shown at the *Top* and *Bottom*, respectively. (*C*) Island-scale semivariograms in the *Inset* graph.

0.37, and 0.34, respectively) on the spatial variation in live coral cover to a depth of 16 m.

Examination of model partial dependency indicated that water depth has a hump-shaped relationship with live coral cover at the scale of the eight MHIs, with maximum cover in the 4- to 8-m range (Fig. 7). This relationship, including a large decrease in the relative importance of water depth on live coral at about 11-m depth, was confirmed during our assessment of patterns within a field validation dataset covering all MHIs from a 2003 coastal habitat mapping project of the National Oceanic and Atmospheric Administration (15). We caution, however, that these trends in controls on live coral only extend to our maximum mapping depth of 16 m, and should not be construed as representing the role of these drivers on deeper corals outside of our mapping capability.

At the scale of the entire eight MHIs, maximum wave power and nearshore development are positively and negatively associated with live coral cover, respectively. Additional factors related to the archipelago-wide geography of live coral cover included sea surface chlorophyll-*a* concentration (positive relationship), average sea surface temperature (negative), and average wave power (positive). It is often said that wave power and live coral cover are negatively related, which was true in our analyses for the islands of Hawai'i, Maui, and Lana'i (*SI Appendix*, Fig. S5). However, that was not true for the islands of Oah'u or Kaua'i, or at the archipelago scale, where repeated bleaching and coastal development have removed large tracts of live coral from leeward areas of low wave power.

Discussion

Our mapping approach reveals intrareef and interreef differences in live coral distributions with implications for a range of conservation and management efforts. First, an archipelago-scale live coral map has the potential to guide coral restoration. Across the MHIs, interisland differences in live coral cover result from a combination of substrate availability related to island age and both land- and reef-use history. Some islands, such as O'ahu, have enormous amounts of reef substrate but are presently dominated by algal cover resulting from the accumulated effects of land and sea use (16). Successful restoration is predicated upon sufficient coral propagation and outplanting combined with mitigation of drivers of ongoing coral loss, particularly those related to reef use and coastal development (17, 18). Coral outplanting alone is a highly complex undertaking currently with limited impact; a global study of more than 500 coral outplants found that only two-thirds survived to the 1-year mark, after which survivorship decreased (8). Given our limited ability to predict where temperatures and water quality will best fit reef restoration, a shortcut could focus on effort in areas with some remaining coral cover, indicating that survival remains viable. Nonetheless, restoration plans must be met with actions to mitigate factors that have reduced live coral cover in the past (19, 20). Our geospatial modeling analysis suggested that, beyond natural factors such as water depth, live coral cover in the Hawaiian Islands is highly regulated by nearshore development.

In parallel to actions undertaken to mitigate negative land–sea impacts on live coral cover, special attention can be focused on the subset of reefs harboring high densities of coral that have thus far survived ocean warming and coastal activity. Our approach identifies these "potential" refugia, with intersite and intrasite comparative data at high resolution at full jurisdictional scale. Doing so affords a ranking of sites based on resilient coral cover as well as reef accessibility, current protections, and land–sea interactions. Underlying causes of living coral resistance likely range from genetics to protective environmental conditions. For example, Kīholo Bay has the highest live coral cover mapped in the MHIs, which coincides with cool subsurface groundwater discharge (21) (*SI Appendix*, Table S1), perhaps affording protection against marine heat waves (22). By contrast, live corals of Pāpā Bay may remain protected on a submerged volcanic shelf with twice the water depth of Kīholo Bay, also providing a thermal refuge. Independent of specific reasons for potential refugia, these maps help generate hypotheses and management-relevant questions for further investigation.

The locations of these potential coral refugia ultimately play a role in determining regional-scale resilience of the entire reef system, particularly in the context of biological source–sink relationships between reefs. Along west Hawai'i Island, for example, reefs with the highest coral cover are widely separated (Figs. 1 and 5). Interspersed among these high coral cover reefs are extensive areas with low-to-moderate coral cover (Fig. 1). Ocean currents are seasonally variable along the west Hawai'i Island coastline, but the predominant flow is latitudinal, with divergence in the north and south directions occurring roughly at the midpoint of the coastal system (*SI Appendix*, Fig. S6). These currents provide reef-to-reef transport of coral, fish, and invertebrate larvae, particularly in surface biological slicks (23). Such biological transport serves as a functional nervous system to the entire reef complex (24), and coral refugia may be contributors to the resilience of this large-scale system.

Patterns of interisland and intraisland variation in live coral cover revealed in our study provide input to resource management and decision-making efforts to conserve remaining areas of high-quality reef, while supporting plans for improving reef resiliency and applying restoration throughout the Hawaiian Islands. In 2016, the State of Hawaii created the Marine 30 × 30

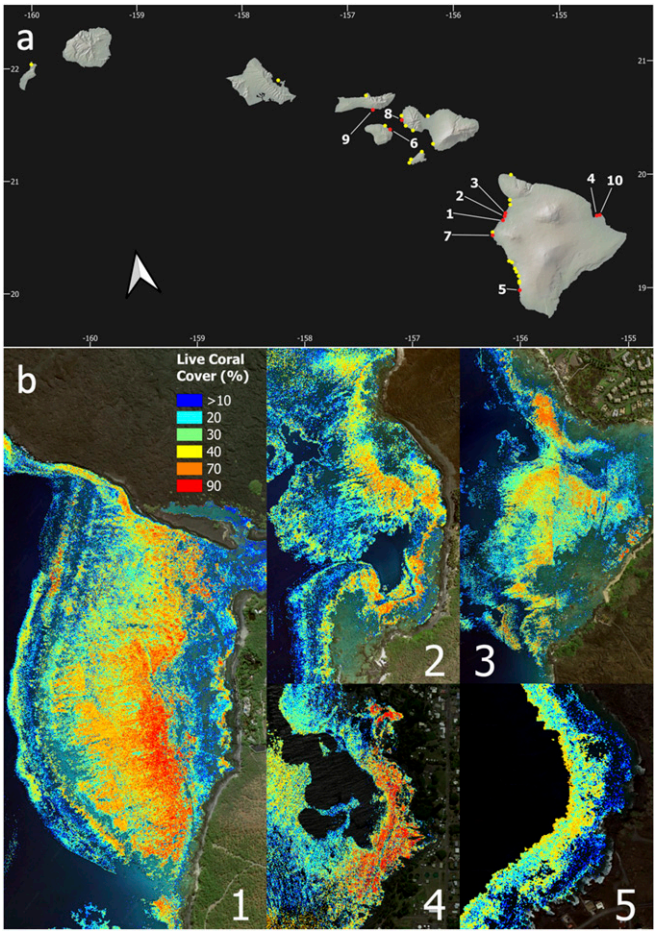

Fig. 5. (*A*) Top 20 reefs (red and yellow dots) based on live coral cover density, with the top 10 (red dots) matching *SI Appendix*, Table S2. (*B*) Zoom maps of the top five live coral cover sites in the Main Hawaiian Islands: (1) Kīholo Bay; (2) Keawaiki; (3) ʻAnaehoʻomalu; (4) Keaukaha; and (5) Pāpā Bay, all of which are on Hawaiʻi Island.

Initiative, an effort to place at least 30% of reefs in the main archipelago into active management (25). Currently, just 6% of reefs are actively managed. The live coral maps assist this initiative in at least three complementary ways. First, marine protections applied to potential coral refugia can create biodiversity banks for the future. Second, areas of moderate live coral cover can be targeted for activities that mitigate land–sea stressors, while planning for large-scale coral reef restoration. Finally, areas of extremely low live coral cover may be difficult to manage using currently available techniques.

High-resolution maps of current live coral cover are a spatially explicit, quantitative baseline against which future conservation performance assessments can be made. Beyond a limited one-time assessment, conservation and management actions will benefit if live coral mapping can be done on a repeat basis. Repeat mapping can improve the determination of coral persistence, particularly to ascertain whether such areas truly constitute formal refugia in the face of land–sea stressors including increased frequency and intensity of marine heat waves (4, 26). Repeat live coral mapping will also help to determine the efficacy of reef management and coral restoration programs. Assessment of net change, both in areas of coral outplanting as well as in comparing outplanting efforts with natural background variability, could assist in applying scarce resources to coral reef management.

The need for continued in situ measurements, whether from traditional fieldwork or camera-based mapping (27, 28), will continue to be central to ensuring the accuracy and interpretation of the large-scale high-resolution live coral mapping we have generated. However, our mapping capability can be repeated at a cost of less than $4 USD per hectare if operated at the scale of the shallow reefs of the entire MHIs. The natural, economic, and cultural significance and value of these reefs, exceeding a billion US dollars per year (29, 30), suggests that large-scale live coral monitoring is warranted in support of management activities intending to increase reef resiliency and ecosystem sustainability.

Methods

Airborne Mapping. We used the Global Airborne Observatory (GAO) (formerly Carnegie Airborne Observatory) (31) to collect mapping data from January 2 to February 4, 2019. To maximize data consistency, airborne operations were performed from 0830 to 1100 local time. To reduce the influence of sky conditions, surface glint, and ocean swells, the coastline covered during each day of operations was determined by monitoring cloud presence and water surface quality. The GAO collected data from multiple coaligned instruments, two of which were used directly for live coral mapping: a high-fidelity visible-to-shortwave infrared (VSWIR) imaging spectrometer and a dual-beam light detection and ranging (LiDAR) scanner (31). In addition, we used a 60-megapixel digital camera to assess and manage sea surface glint levels during flight. A precise position and orientation system enabled the computation of aircraft trajectory to within 5 cm (RMSE) during all flights. Global Positioning System (GPS) timing data were collected during flight by all three instruments, and this information, along with known position and instrument boresight offsets, allowed precise back-computation of position and orientation for the receiver of each instrument.

During flight, instrument settings were set for the planned nominal flight altitude of 2 km above the sea surface. Flightlines were spaced to achieve 50% overlap in VSWIR spectrometer coverage. Aircraft groundspeed was 130 to 140 kt. LiDAR pulse frequency was set to 200 kHz (100 kHz per laser) and scan frequency was 34 Hz with a field of view of 38°, allowing 2° of buffer on each side of the spectrometer field of view of 34°, achieving a nominal pulse density of more than 4 pulses·m^{-2}. The digital camera provided more than 60% side overlap between flightlines.

Data Processing. After airborne collection, data from all three instruments were orthorectified and both radiometrically and atmospherically corrected. The raw LiDAR point cloud data were converted to a 1-m resolution digital surface model (DSM) by interpolating between the first returns from each pulse. A sufficient number of returns from the infrared (1,064 nm) LiDAR beams reflected by the water surface were recorded to allow the production of an interpolated water surface elevation map.

The VSWIR spectrometer sampled at a rate of 100 frames·s^{-1}. The raw spectrometer data collected onboard the GAO were first converted to radiance using laboratory calibration data collected before the campaign. The radiance data contain 427 spectral channels covering the wavelengths between 350 and 2,500 nm in 5-nm increments. With the LiDAR DSM and known position, orientation, and camera lens model for each instrument, the three-dimensional position of each spectrometer and digital camera pixel was ray-traced to the sea surface level. Using the LiDAR-derived observation angles and elevation as inputs, we performed atmospheric correction with a modified version of the ATREM model (32, 33).

Orthorectification of each flight line was adjusted for water refraction and depth. We used a neural network deep learning model to compute depth for each flight line (34). Then for each spectrometer pixel, the at-surface view zenith angle, φ_a, was modified for refraction at the air–water interface to get below-surface zenith angle, φ_b, using Snell's law and standard refractive indices for water and air, respectively. From the original sea surface location, this angle was traced to the modeled ocean floor depth to get a new three-dimensional position for each spectrometer pixel representing the pixel location on the seafloor. With the location of each spectrometer pixel known, individual flight lines were mosaicked together using a strategy of minimum glint, where glint is defined as the average reflectance value for the five spectral bands covering the wavelengths 890 to 910 nm for each pixel. For each mosaic map pixel location, data from the flight line with the lowest glint at that location was kept.

Model Training Data. Training data for the deep learning model were taken from multiple sources. We collected 979 RTK-GPS field points along the West

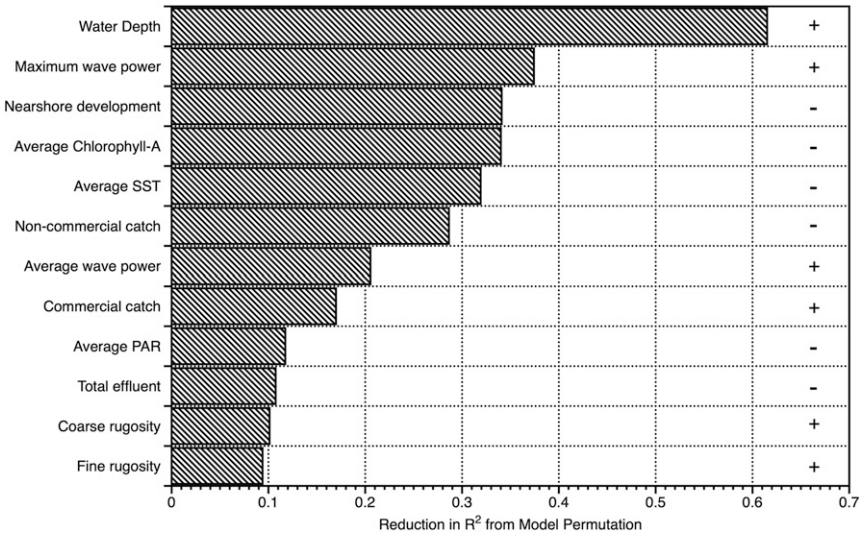

Fig. 6. Relative importance of factors related to live coral cover throughout the eight Main Hawaiian Islands. PAR, photosynthetically active radiation; SST, sea surface temperature. Plus (+) and minus (–) symbols indicate the relationship of the driver variable with live coral cover. See *SI Appendix*, Table S1 for model data information.

Coasts of Hawai'i, Maui, and O'ahu, each identifying a point over a live coral- or algal-dominated surface. In addition, 36,067 points were added from imagery over clear and obvious sand and nonbenthic objects such as low clouds, breaking waves, and surface-exposed bare rock. We also incorporated high live coral cover from field-based transect data, described in the next section. While the positioning of the transect data was not precise enough to use as point inputs to the deep learning model, spectrally uniform areas under some of these transects were outlined ($\leq 10 \times 10$ m), and reflectance spectra were averaged within these regions and given the live coral cover value for the given transect. This was done for 208 transects, which were partitioned by percentage of live coral cover as follows: 30 at 0%, 192 at 5%, 37 at 5 to 25%, 18 at 25 to 50%, and 31 at >50%.

In a similar manner, we used publicly available validation data from a coastal habitat mapping project of the National Oceanic and Atmospheric Administration (15). These 3,021 samples were collected by divers, underwater viewers, and drop cameras at locations across all Hawaiian Islands. The positional accuracy of these data as well as the temporal delay since collection precluded their use directly as point training data for this model. Again, spectrally uniform areas from 124 of the points were averaged and assigned the proportional cover types in the dataset. These points were partitioned by percentage of live coral as follows: 77 at 0%, 14 at 10%, 15 at 20 to 30%, 21 at 40 to 50%, and 42 at >50%.

Model Training. We used the TensorFlow package in Python (35) to train a feed-forward neural network model with 150 VSWIR spectrally contiguous bands of reflectance data (380 to 1,130 nm to distinguish both benthic and nonbenthic targets) as well as matching GAO depth as input. The model architecture included a 151-node input layer, along with three dense hidden layers of 2,000, 2,000, and 500 nodes, respectively, with a dropout layer of ratio 0.2 between each of the hidden layers. All dense hidden layers used a RELU activation function. Finally, a four-node output layer was used, one each for proportion of sand, live coral cover, algal cover, and "other," using a sigmoid activation function. Here, algal cover is defined as a combination of strong light-absorbing turf algae and weaker light-absorbing macroalgae. This final sigmoid activation function ensured that the output values for each class ranged from 0.0 to 1.0. However, this did not force the sum total of the four classes' predictions to be 1 (or 100% cover). Because of the unbalanced training data and the need for the four outputs to sum to unity, we created a custom loss function that returned a sum of three components:

1. A weighted mean square error (MSE) across all classes, with class weights 1.10, 1.10, 0.95, and 0.85 for sand, live coral cover, algal cover, and "other," respectively:

$$\frac{\sum_{i\in 1..n, j\in 1..m} w_j \left(\hat{y}_{ij} - y_{ij}\right)^2}{nm}.$$

2. A penalty for sums not totaling 1:

$$\sum_{i\in 1..n} \left(\sum_{j\in 1..m} y_{ij} - 1 \right)^2.$$

3. An extra 2 × MSE penalty for prediction errors of training points with 100% cover in any of the classes, i.e., highly confident training samples:

$$\frac{2}{n} \cdot \sum_{i\in 1..n} \begin{cases} \left(\hat{y}_{ij} - y_{ij}\right)^2, & \max_{j\in 1..m} y_{ij} = 1.0 \\ 0, & \max_{j\in 1..m} y_{ij} \neq 1.0 \end{cases}.$$

During model execution, 80% of the above-described field data were used for training, and 20% were used as stopping criteria and test set. We used the ADAM optimization algorithm (36) to fit the network coefficients to the training data, with an automatic stop determined as no improvement in the validation set loss value in 15 epochs. The model required 156 epochs to reach this optimization criterion, with the overall unweighted MSE across all classes settling at 0.0324. Individual class MSE values from the test set were 0.0355, 0.0314, 0.0383, and 0.0083 for the sand, live coral cover, algal cover, and "other" classes, respectively.

Maps of live coral, algal cover, and sand cover were derived for more than 95% of reefs of the MHIs to a depth of 16 m. These maps were mosaicked for each of the MHIs at 2-m resolution. When applied at full MHI scale, spectroscopic errors due to atmospheric and water anomalies (rough and high turbidity conditions) caused some noticeable coral overprediction artifacts from the model extrapolating. To mitigate these artifacts, a second Gradient Boosting Model (GBM) (37) was used solely as a check on the live coral cover prediction results from the neural network model. Training and testing of the GBM were carried out with the same input data using the same training/validation split used for the network model, with the exception that only the live coral cover values were used as a response variable. The GBM was performed using the Scikit-Learn Python package (38) with the number of regressors set to 500 (determined using a grid search optimization approach). Other model metaparameters were left at their default values. The MSE for live coral cover on the test set was 0.0386, which was higher than the neural network model, and the predicted live coral cover was generally lower in the GBM than the neural network model. However, visual assessment of output maps suggested that patterns of live coral cover were sufficiently similar between maps and, importantly, the GBM model lacked overprediction

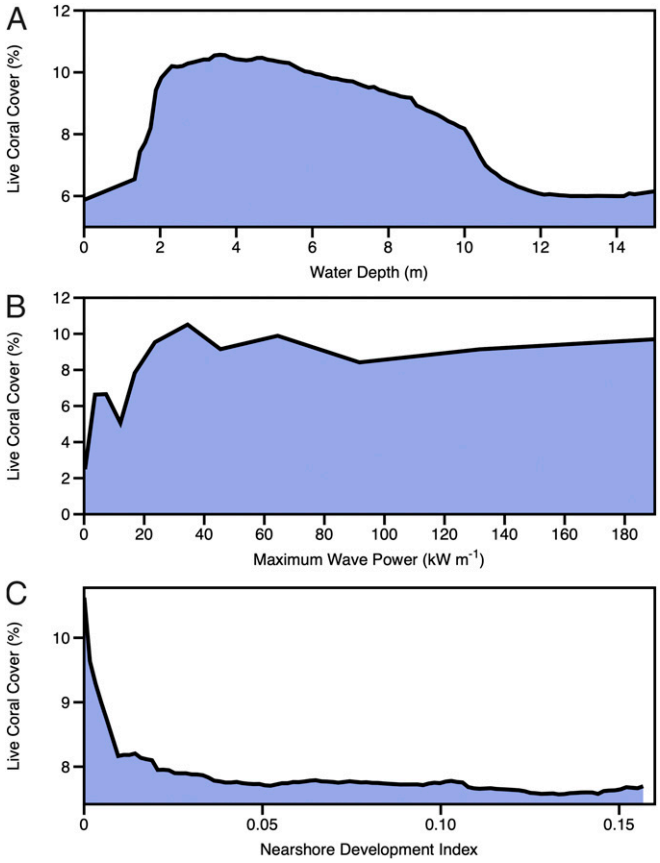

Fig. 7. Partial dependency plots showing relative differences in live coral cover for the top three land–sea drivers in our analysis from Fig. 6. (*A*) Water depth; (*B*) maximum wave power; and (*C*) an index of nearshore development index.

artifacts in the same places. Thus, the GBM maps could serve well as a check for overprediction artifacts in the neural network model-based maps.

Maps with most artifacts removed were produced using the following function of the live coral values from the two models, using a cutoff value for the difference between the models of 0.65 that was determined by iteration:

$$y_c' = \begin{cases} y_{c,NN}, & y_{c,NN} < y_{c,GBM} + 0.65 \\ y_{c,GBM}, & \text{otherwise} \end{cases}.$$

When predicted live coral value was changed in this way, the reduction in cover, $y_{c,NN} - y_{c,GBM}$, was reallotted proportionally to the other three classes, sand (*s*), algal (*m*), and "other" (*o*) based on their previous contribution to the total cover of the given pixel, i.e., the following:

$$y_i' = y_i + \frac{y_i}{\sum_{\{s,m,o\}} y_i} \cdot \left(y_{c,NN} - y_{c,GBM}\right) \qquad \forall i \in [s, m, o].$$

Field Validation. From August to November 2019, we carried out diver-based transect surveys to assess error in mapped live coral cover estimates. At each site, we conducted one 25-m transect along three isobaths of 5-, 10-, and 15-m depth. When deeper isobaths were not possible, we generated transect replicates at available isobaths at each site. Divers recorded benthic composition every 0.25 m to species level for living taxa and recorded all nonliving substrate. We took GPS coordinates at the start and end of each transect with a Garmin eTrex 30x (Garmin Ltd.). An Arizona State University (ASU) set of 129 transects on Hawai'i Island had a depth breakdown of <5 m (n = 2), 5 to 10 m (n = 48), 10 to 15 m (n = 49), and >15 m (n = 30) (*SI Appendix*, Fig. S3). These transects generated 129 mean live coral cover estimates that were geospatially aligned with the airborne imaging spectrometer data.

In addition to ASU field data, we also incorporated transect data collected in October to November 2019 by the Hawai'i Department of Land and Natural Resources, Division of Aquatic Resources (DAR). The DAR data were also collected using 25-m transects at depths ranging from <5 to >15 m on the islands of Hawai'i (n = 28), Maui (n = 297), Moloka'i (n = 29), and O'ahu (n = 649). The depth breakdown of the DAR data were <5 m (n = 763), 5 to 10 m (n = 153), 10 to 15 m (n = 86), and >15 m (n = 1). The DAR transects were also located using handheld GPS units, and the data were averaged by transect to generate a total of 1,003 live coral cover estimates for comparison to the airborne data. Combined, the ASU and DAR data totalled 1,132 transects on four islands (*SI Appendix*, Fig. S3).

Geospatial Analyses. We next assessed the spatial patterning of live coral between and within the MHIs using empirical variograms. We broke the live coral map for each island into a grid of 500 × 500 pixels (1-km) cells. Because of the additive nature of the variogram variances, we computed one for each island using sample-size weighted averages of the individual lag variances across grid cells into a single variogram. This methodology provided the additional benefit of generating information about the variation in spatial patterning within each island. For each 1-km grid cell, an empirical variogram was computed with the GeoStats package (39) in the Julia programming language (40), using 40 lag steps and a maximum lag of 500 m. A variogram model was fit to the empirical variogram for each grid cell to derive sill, nugget, and range parameters. An island-wide empirical variogram was computed as a weighted average of the variograms from all grid cells from that island, where the weight for each cell was the number of valid live coral observations separated by the given lag distance within that cell.

Land–Sea Driver Modeling. We used 14 land–sea environmental maps available for the MHIs to assess the relative importance of environmental and human factors on the mapped distribution of live coral (*SI Appendix*, Table S2). These maps included the water depth and three benthic surface metrics derived from the GAO (34): planar curvature computed using a 3 × 3 pixel (6 × 6-m) moving window, "fine" planar rugosity computed using a 9 × 9 pixel (18 × 18-m) moving window, and "coarse" planar rugosity computed after upscaling the depth data to 6 m with a mean filter, using a 9 × 9 pixel (54 × 54-m) moving window (41). We also used several datasets derived by the Ocean Tipping Points project (9): average and maximum ocean wave power (42); average annual commercial and noncommercial fishing catch (43); nearshore development (44); average and maximum sea surface temperature (45); average photosynthetically active radiation (PAR) and chlorophyll-*a* concentration (46); and total pollutant effluent (9). We tested the validity of including sea surface temperature anomalies and degree heating weeks as potential drivers of 2019 live coral cover. We found that the massive 2015 marine heat wave dominated the temperature anomaly maps, and that event had also dominated the eastern side of the MHIs (Hawai'i and Maui) where coral cover is naturally higher (*SI Appendix*, Fig. S7). This generated a spurious result relating higher temperatures to higher coral cover on the time and space scale of this study.

To better match the resolution of these land-sea factors, the GAO live coral cover maps were coarsened to 30-m resolution using a mean filter. All input factors were resampled to match this resolution using cubic spline interpolation. We randomly selected 80,000 30-m pixels from the eight MHI coastlines, covering 7,200 ha of mapped reef, to carry out the modeling analyses. Modeling was carried out using a Random Forest Machine Learning approach (47) with the Scikit-Learn Python package (38). A full grid search was performed to find the best metaparameters for the model, and the optimal settings were 2,000 estimators, one sample per leaf, two samples per split, and four features scanned at each split. This model achieved an R^2 = 0.90. We assessed the importance of each variable using a permutation-based, R^2-reduction metric. For each input variable, for each of five iterations the values for this variable were randomly shuffled, keeping values of all other variables intact. Model predictions were performed using the permuted dataset, and we retained the difference between the original R^2 (0.90) and the R^2 computed from this permutation. The five difference values were averaged for each variable to get a single importance value, where larger positive values indicate greater reduction in R^2 and, equivalently, greater variable importance.

Data Availability. Digital mapping data are currently available on Zenodo (http://doi.org/10.5281/zenodo.4292660) (48). All study data are included in the article and *SI Appendix*.

ACKNOWLEDGMENTS. We thank colleagues from the Division of Aquatic Resources, Hawaii State Department of Land and Natural Resources, for their field data collection efforts on four islands. We thank B. Grady for auditing the live coral maps. This study was supported by the Lenfest Ocean Program and The Battery Foundation. The Global Airborne Observatory is made possible with support of private foundations, visionary individuals, and Arizona State University.

1. T. P. Hughes *et al*., Coral reefs in the Anthropocene. *Nature* **546**, 82–90 (2017).
2. O. Hoegh-Guldberg *et al*., Coral reefs under rapid climate change and ocean acidification. *Science* **318**, 1737–1742 (2007).
3. T. Kutser, J. Hedley, C. Giardino, C. Roelfsema, V. E. Brando, Remote sensing of shallow waters—a 50 year retrospective and future directions. *Remote Sens. Environ.* **240**, 111619 (2020).
4. G. Keppel, G. W. Wardell-Johnson, Refugia: Keys to climate change management. *Glob. Change Biol.* **18**, 2389–2391 (2012).
5. G. Keppel *et al*., The capacity of refugia for conservation planning under climate change. *Front. Ecol. Environ.* **13**, 106–112 (2015).
6. C. Cacciapaglia, R. van Woesik, Reef-coral refugia in a rapidly changing ocean. *Glob. Change Biol.* **21**, 2272–2282 (2015).
7. R. van Hooidonk *et al*., Local-scale projections of coral reef futures and implications of the Paris Agreement. *Sci. Rep.* **6**, 39666 (2016).
8. S. A. Foo, G. P. Asner, Sea surface temperature in coral reef restoration outcomes. *Environ. Res. Lett.* **15**, 074045 (2020).
9. L. M. Wedding *et al*., Advancing the integration of spatial data to map human and natural drivers on coral reefs. *PLoS One* **13**, e0189792 (2018).
10. J.-B. Jouffray *et al*., Parsing human and biophysical drivers of coral reef regimes. *Proc. Biol. Sci.* **286**, 20182544 (2019).
11. K. S. Rodgers, K. D. Bahr, P. L. Jokiel, A. Richards Donà, Patterns of bleaching and mortality following widespread warming events in 2014 and 2015 at the Hanauma Bay Nature Preserve, Hawai'i. *PeerJ* **5**, e3355 (2017).
12. V. E. Neall, S. A. Trewick, The age and origin of the Pacific islands: A geological overview. *Philos. Trans. R. Soc. Lond. B Biol. Sci.* **363**, 3293–3308 (2008).
13. P. J. Mumby *et al*., The cover of living and dead corals from airborne remote sensing. *Coral Reefs* **23**, 171–183 (2004).
14. M. Dornelas *et al*., Quantifying temporal change in biodiversity: Challenges and opportunities. *Proc. Biol. Sci.* **280**, 20121931 (2013).
15. M. S. Coyne *et al*., "Benthic habitats of the main Hawaiian islands" (Technical Memorandum NOS NCCOS CCMA 152, National Oceanic and Atmospheric Administration, 2003).
16. J. M. Pandolfi *et al*., Ecology. Are U.S. coral reefs on the slippery slope to slime? *Science* **307**, 1725–1726 (2005).
17. M. C. Ladd, A. A. Shantz, Trophic interactions in coral reef restoration: A review. *Food Webs* **24**, e00149 (2020).
18. S. E. Lester, A. K. Dubel, G. Hernán, J. McHenry, A. Rassweiler, Spatial planning Principles for marine ecosystem restoration. *Front. Mar. Sci.* **7**, 328 (2020).
19. J. A. Hollarsmith, S. P. Griffin, T. D. Moore, "Success of outplanted *Acropora cervicornis* colonies in reef restoration" in *Proceedings of the 12th International Coral Reef Symposium*, D. Yellowlees, T. P. Hughes, Eds. (James Cook University, Townsville, QLD, Australia, 2012), ICRS2012_20A_3.
20. S. A. Schopmeyer *et al*., Regional restoration benchmarks for *Acropora cervicornis*. *Coral Reefs* **36**, 1047–1057 (2017).
21. A. G. Johnson, C. R. Glenn, W. C. Burnett, R. N. Peterson, P. G. Lucey, Aerial infrared imaging reveals large nutrient-rich groundwater inputs to the ocean. *Geophys. Res. Lett.* **35**, L15606 (2008).
22. R. N. Peterson, W. C. Burnett, C. R. Glenn, A. G. Johnson, Quantification of point-source groundwater discharges to the ocean from the shoreline of the Big Island, Hawaii. *Limnol. Oceanogr.* **54**, 890–904 (2009).
23. J. M. Gove *et al*., Prey-size plastics are invading larval fish nurseries. *Proc. Natl. Acad. Sci. U.S.A.* **116**, 24143–24149 (2019).
24. J. Miller, "Nearshore distribution of Hawaiian marine fish larvae: Effects of water quality, turbidity and currents" in *The Early Life History of Fish*, J. H. S. Blaxter, Ed. (Springer, 1974), pp. 217–231.
25. Department of Land and Natural Resources, "Marine 30x30 initiative" in *Achieving Effective Management in 30% of Hawai'i's Nearshore Waters by 2030* (Department of Land and Natural Resources, Hawaii, 2019).
26. E. C. J. Oliver *et al*., Longer and more frequent marine heatwaves over the past century. *Nat. Commun.* **9**, 1324 (2018).
27. J. Burns, D. Delparte, R. D. Gates, M. Takabayashi, Integrating structure-from-motion photogrammetry with geospatial software as a novel technique for quantifying 3D ecological characteristics of coral reefs. *PeerJ* **3**, e1077 (2015).
28. V. Chirayath, R. Instrella, Fluid lensing and machine learning for centimeter-resolution airborne assessment of coral reefs in American Samoa. *Remote Sens. Environ.* **235**, 111475 (2019).
29. C. D. Storlazzi *et al*., "Rigorously valuing the role of U.S. coral reefs in coastal hazard risk Reduction" (Open-File Report 2019-1027, US Geological Survey, 2019).
30. R. C. Bishop *et al*., "Total economic value for protecting and restoring Hawaiian coral reef ecosystems: Final report (NOAA Technical Memorandum CRCP 16, Office of National Marine Sanctuaries, and Coral Reef Conservation Program, NOAA, Silver Spring, MD, 2011), p. 406.
31. G. P. Asner *et al*., Carnegie Airborne Observatory-2: Increasing science data dimensionality via high-fidelity multi-sensor fusion. *Remote Sens. Environ.* **124**, 454–465 (2012).
32. B.-C. Gao, A. F. H. Goetz, Column atmospheric water vapor and vegetation liquid water retrievals from airborne imaging spectrometer data. *J. Geophys. Res.* **95**, 3549–3564 (1990).
33. D. R. Thompson *et al*., Airborne mapping of benthic reflectance spectra with Bayesian linear mixtures. *Remote Sens. Environ.* **200**, 18–30 (2017).
34. G. P. Asner, N. R. Vaughn, C. Balzotti, P. G. Brodrick, J. Heckler, High-resolution reef bathymetry and coral habitat complexity from airborne imaging spectroscopy. *Remote Sens.* **12**, 310 (2020).
35. M. Abadi *et al*., Tensorflow: Large-scale machine learning on heterogeneous distributed systems. arXiv:1603.04467 (14 March 2016).
36. D. Kingma, J. Ba, Adam: A method for stochastic optimization. arXiv:1412.6980 (22 December 2014).
37. L. Mason, J. Baxter, P. L. Bartlett, M. R. Frean, "Boosting algorithms as gradient descent" in *Advances in Neural Information Processing Systems 12*, S. A. Solla, T. K. Leen, K.-R. Müller, Eds. (MIT Press, 2000), pp. 512–518.
38. F. Pedregosa *et al*., Scikit-learn: Machine learning in Python. *J. Mach. Learn. Res.* **12**, 2825–2830 (2011).
39. J. Hoffimann, GeoStats.jl—high-performance geostatistics in Julia. *J. Open Source Softw.* **3**, 692 (2018).
40. J. Bezanson, S. Karpinski, V. B. Shah, A. Edelman, Julia: A fast dynamic language for technical computing. arXiv:1209.5145 (24 September 2012).
41. J. S. Jenness, Calculating landscape surface area from digital elevation models. *Wildl. Soc. Bull.* **32**, 829–839 (2004).
42. N. Li *et al*., Thirty-four years of Hawaii wave hindcast from downscaling of climate forecast system reanalysis. *Ocean Model.* **100**, 78–95 (2016).
43. K. S. McCoy *et al*., Estimating nearshore coral reef-associated fisheries production from the main Hawaiian islands. *PLoS One* **13**, e0195840 (2018).
44. Center for International Earth Science Information Network, Gridded Population of the World, Version 4 (GPWv4): Population Count (Center for International Earth Science Information Network, Columbia University, 2020).
45. A. Ignatov, GOES-R Advanced Baseline Imager (ABI) Algorithm Theoretical Basis Document for Sea Surface Temperature (NOAA NESDIS Center for Satellite Applications and Research, 2010).
46. NASA Goddard Space Flight Center, Ocean Biology Processing Group, Sea-Viewing Wide Field-of-View Sensor (SeaWiFS) Ocean Color Data (Active Archive Center [OB.DAAC], Goddard Space Flight Center, Greenbelt, MD, 2014). doi.org/10.5067/ORBVIEW-2/SEAWIFS_OC.2014.0. Accessed 15 January 2020.
47. L. Breiman, Random forests. *Mach. Learn.* **45**, 5–32 (2001).
48. G. P. Asner, N. Vaughn, J. Heckler, Global airborne observatory: Hawaiian Islands live coral cover in 2019 (Version 3.0). *Zenodo*. http://doi.org/10.5281/zenodo.4292660. Deposited 26 November 2020.